Chapter 4

THE CONTINUOUS-GUST AND QUASI-COHERENT TURBULENT VELOCITY FIELD

To account for the transient effects of gustiness, the random (or at least less-organized) nature of wind motions is leveraged to consider a stationary time series whose statistics can be regarded as constant and independent of the origin of time when averaged over a suitable time period (say, five minutes to an hour). With these statistics in hand, the task becomes one of simulation of suitable forcing spectra for the regions of interest during anticipated times-of-flight. That is to say that to experimentally simulate the continuous-gust turbulent velocity field a flyer is likely to experience far above, just above or at times, within the canopy layer, one must produce time records in a wind tunnel that exhibit the statistical characteristics and sequential behavior of the actual turbulence in the region during the times of flight. Because it is not currently possible to simulate the full range of relevant atmospheric motions for every stability condition in a laboratory setting, special emphasis is placed on representative energetic disturbances near the surface that overlap frequencies of note in the flyer response spectrum during the presence of a reasonably strong wind. An example of simulation of the gusty region just above the canopy top in the roughness sublayer was briefly mentioned in fig. 2.7 in the context of generation of unsteady flowfields. As will be seen, this unsteadiness calls into question the applicability of the following statistical analysis so unsteady flowfields initiated by the 'breathing' modality are omitted in this chapter and left to future careful study. The remaining two instances, however, will be considered in depth, namely the spectral overlap of atmospheric turbulence far above local effects in the inertial sublayer and the superimposed wake region within the canopy layer.

4.1 Turbulence-generation techniques in wind tunnels

Conventional wind tunnel turbulence-generation techniques

Passive grid-generated turbulence remains the stalwart experimental technique to develop isotropic turbulence in a wind tunnel. The technique is considered passive insomuchas the grid acts as a geometric obstacle to the flow and is not itself vibrating, rotating, or otherwise adding mean momentum to the flow. Resulting turbulence energy decays according to the law of the so-called initial-period-of-decay that is

valid beyond the first 30 mesh lengths over a wide range of Reynolds numbers (e.g., see Loehrke and Nagib, 1972). The generated turbulence is insensitive to most grid design parameters other than solidity. Use of a contraction further showed improved isotropy (Comte-Bellot and Corrsin, 1966) and has become a staple element of closed-return wind tunnel design ever since. Passive grid-generated turbulence in conventional wind tunnels results in typical values of $Re_{\lambda_T} \sim 50 - 150$.

In light of the experimental findings of Sheih et al. (1971) in the ABL, a push to increase turbulence Reynolds numbers through active means was initiated by many researchers (e.g. Gad-el-Hak and Corrsin, 1974). Arguably the most successfully-implemented active turbulence generation technique in wind tunnels to-date is based on the grid design of Makita (1991), where $Re_{\lambda_T} \sim 400$ was achieved in a relatively small wind tunnel (0.7×0.7 m^2) with a mean velocity of 5 m/s. Roadman and Mohseni (2009, Table A1) gives a rather exhaustive list of wind- and water-tunnel-generated turbulence with both active and passive grids and a supplemental list of the various Makita-style active grids to-date is given by Hearst (2018, Table 1).

Turbulence-generation techniques using multi-source wind tunnels

Multi-source wind tunnels can generate active turbulence through shearing velocities initialized at the fan array exit plane through software-enabled reconfigurations alone[1] . In the random-phase (R-P) mode, inlet conditions are initialized out-of-phase and driven sinusoidally such that velocity ratios of adjacent input increments are always changing in time and taking a pseudo-random value between zero and one. This reduces the prevalence of any specific shear-induced length scale to be encountered downstream in the measurement domain. In contrast, the quasi-grid (Q-G) configuration is presented as a static software assignment of alternating on-off patterns such that the velocity ratio at each on-off interface is always constant (and maximally one). A specific wake-like geometric length scale is introduced at the array exit plane accordingly and a shear-induced length scale may persist downstream in the measurement domain. Combinations of these techniques are also possible.

[1]Of course any of the traditional geometric turbulence (hardware) augmentation techniques can be implemented instead-of or in-addition-to, but the effect of software augmentation alone on the inlet conditions is exclusively explored herein.

Random-phase (R-P) mode

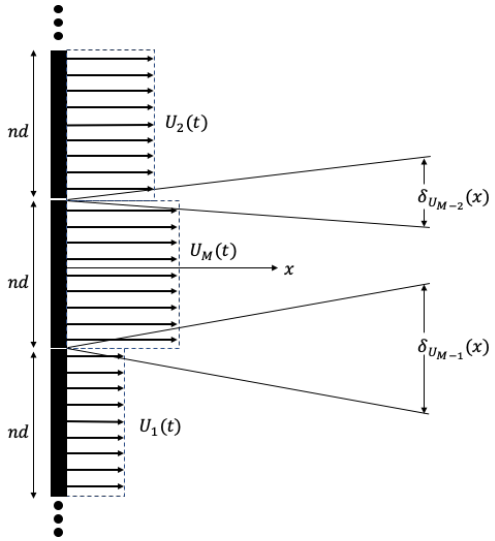

$(0 < \Delta U(t)/2\overline{U}(t) < 1)$

Quasi-grid configuration

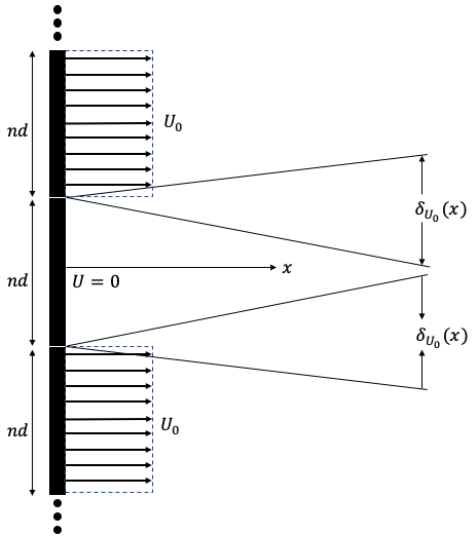

$(\Delta U/2\overline{U} = C = 1$, as drawn)

Figure 4.1: Conceptual drawing of shearing velocities initiated at the fan array exit plane.

4.2 Analysis techniques

Though a turbulent flow can vary in all three spatial dimensions in time, a one dimensional spectra is oftentimes used to describe the way in which waves, or eddies, exchange energy along the most practically measurable dimension of information. Time-based point measurements can be correlated to a time-lagged version of itself (autocorrelation) and subsequently Fourier-transformed into the frequency domain to generate a so-called one-dimensional energy spectra. Because measurements along a line cannot distinguish between wavenumber vectors aligned with the direction of measurement from those oblique to the direction of measurement, wavenumbers higher than a given wavenumber value $k/2\pi = f/\overline{u}$ contribute energy to that particular wavenumber in a process called aliasing. Thus, there presents a finite energy value at $k = 0$ proportional to an integral length scale L_{11} in a one-dimensional energy spectra when physically there should be no energy at this value. For a quasi-steady velocity field, the contribution from all frequencies to the one-dimensional energy spectrum sums to the total energy, given as a constant average value satisfying the condition:

$$\int_0^\infty E_{11}(f)\, df = \overline{u'^2} \tag{4.1}$$

where $E_{11}(f)$ describes the fluctuating energy of the u-component of motion per unit frequency at the frequency f. Because energy spans over a broad range of scales for atmospheric flows, it is customary to plot the abscissa of the spectra on a logarithmic scale. By using the relation

$$\int_0^\infty E_{11}(f)\, df = \int_0^\infty f \cdot E_{11}(f)\, dln(f) \tag{4.2}$$

spectra plotted as $fE_{11}(f)$ vs $ln(f)$ preserves the relation that the area under the curve represents variance of energy, as in eq. (4.1), and further preserves its magnitude when converting from the frequency domain to the wavenumber domain when Taylor's hypothesis holds, since $fE_{11}(f) = kE_{11}(k)$. Where temporal wind records are characterized by a time-varying mean velocity, length scale statistics are omitted and left to future careful study. For the temporal wind records with rather steady mean velocities generated herein, Taylor's hypothesis is deemed reasonable, and the Taylor microscale, is calculated from:

$$\lambda_T^2 = \frac{\overline{u}^2 u'^2}{\overline{(\frac{\partial u}{\partial t})^2}} \tag{4.3}$$

The frequencies of interest

Given the inherent variability of the flow regimes that are candidates for simulation, it is useful to set functional limits ranged upon the frequencies of interest. Panofsky and McCormick (1954), using time series measured at $z = 100$ m at the Brookhaven National Laboratory site that would later be used to generate the spectrum of fig. 1.7, gives a conservative estimate that at frequencies on the order of about 1 Hz and greater, the spectral intensity does not depend on radiation intensity but is proportional to the square of the mean wind speed. The explicit threshold provided (a reduced frequency of $fz/\overline{u} < 0.6$) suggests convection may only play an important role in the production of eddies with periods of about 30 seconds and longer ($f \approx 0.03$ Hz and lower). As such, any forcing function with forcing frequencies less than $f_f = 0.05$ Hz will not be considered as a suitable candidate for mechanical-type turbulence simulation and are thus excluded. A further narrowing of frequencies of interest above canopies is possible if we are to consider, as an example, a canopy with average roughness element height of, say, 25 m within a 500 m neutrally-stratified boundary layer depth. The wind tunnel studies referenced in section 1.6 suggest longitudinal length scales ranging from order 10^0 m to 10^1 m based on $H = 25$ m. For nominal mean velocities of reasonably strong winds, then the frequencies of peak energy would fall within the range of $0.1 < f_p < 0.5$ Hz. Any forcing function initiated discretely in time intending to simulate an unsteady gusty environment will be limited to this range.

4.3 Experimental simulation results and discussion

Spectral results for the many candidate turbulent flowfields tested are provided in the dimensional frequency domain. Those with steady mean velocity are further analyzed in the wavenumber domain. This phase of experimentation focused on the great many combinations of flowfield inputs available through software augmentation, and as such one single-wire hotwire testing apparutus was fixed along the centerline at $x/d \sim 30$ $(x/nd = x/L \sim 0.8125, n = 36)$, sampling at 2 kHz for either 32 or 64 seconds per experiment. Streamwise and spanwise traversals are set for future work, so no direct statement of homogeneity is provided at this time.

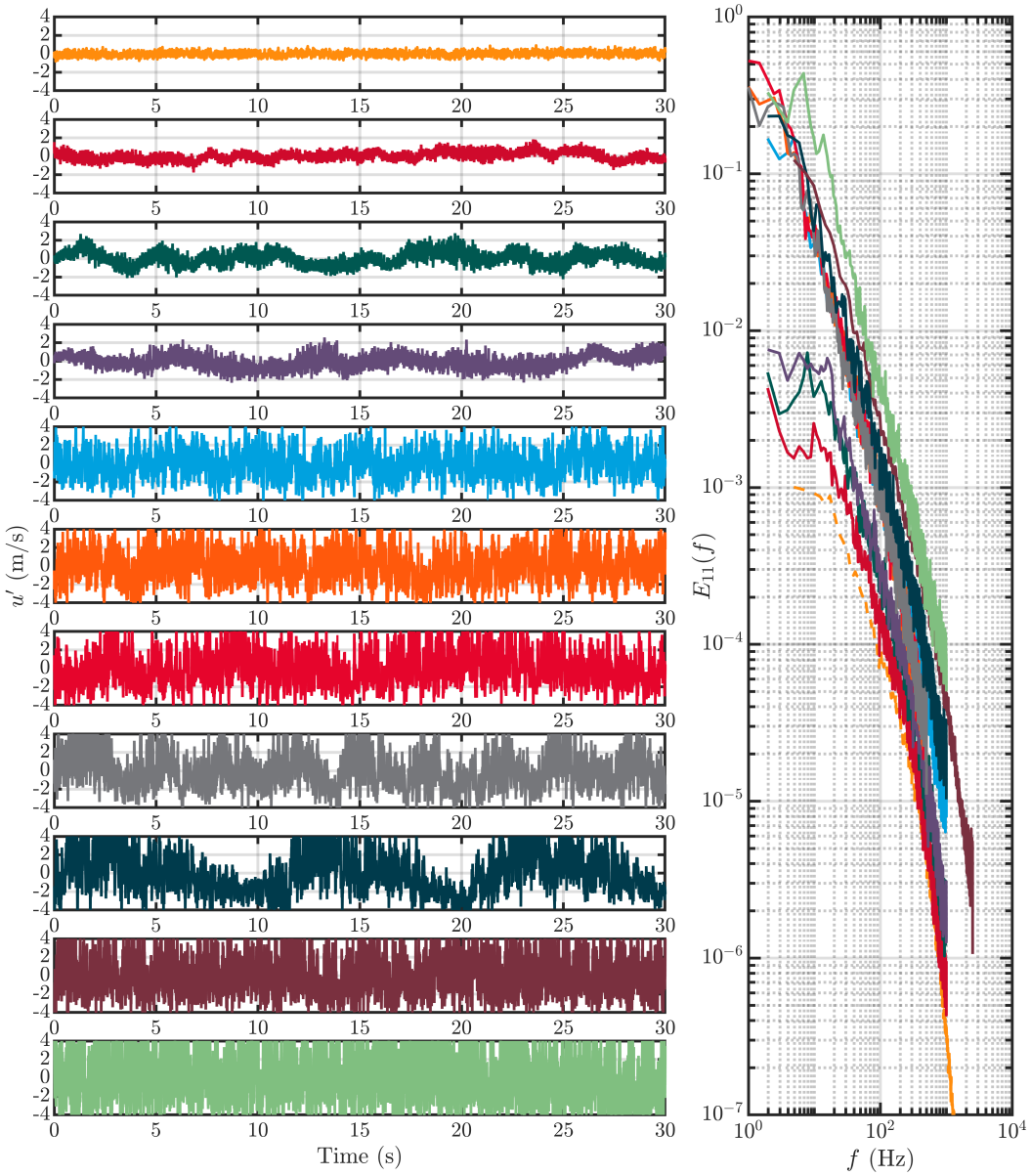

Figure 4.2: Fluctuating component time series and corresponding u-spectra in the frequency domain for the measured turbulent flowfields.

Results - random-phase and quasi-grid

Figure 4.3 showcases the u-spectra of a selection of measured flowfields with steady mean velocity profiles. The uniform turbulent flowfield generated when all fans are specified to the same input condition (i.e. the uniform flow modality) is considered to be the baseline flowfield and is drawn as dashed when included. The Taylor

microscale Reynolds number for this baseline case is $Re_{\lambda_T} = 135$, which falls within range of typical passive grid-generated wind tunnel turbulence, and decays with downstream evolution according to fig. A.5 and fig. A.10. A range of $500 \lesssim Re_{\lambda_T} \lesssim 900$ is achieved by activating the random-phase (R-P) mode to the baseline case, where the mean velocity is maintained at $\overline{u} = 8.1 \pm 0.3$ m/s, and the turbulence intensity increases from $TI = 5.4\%, 8.3\%, 9.6\%$ for a commanded 30%, 50%, 90% allowable ranged fluctuation amplitude away from the prescribed mean velocity input, respectively. A near doubling of Re_{λ_T} is achieved by spatially partitioning the array into a so-called quasi-grid (Q-G) configuration. Intergrid spacing is initialized with $l_g = nd = 0.320$ m ($n = 4$) in each direction (i.e. adjacent 4x4 blocks of fans alternate on-off-on-off in a gridded manner), resulting in a ratio of deactivated module area to total fan array area, or effective solidity, of $\wp = 69.1\%$.

Discussion - turbulence generation by shearing

Though the mechanisms of the generation of turbulence effect the nature of the spectra of a flowfield in the low-wavenumber regions, the phenomenological theory put forth by Kolmogorov (1941) presumes that the behavior of the scale motions over an intermediate range of scales in the inertial subrange smaller than the largest eddy length scale but larger than the dissipation length scale η is governed by a constant dissipation rate with a spectrum of the shape $E(k) = C_k \epsilon^{2/3} k^{-5/3}$, assumed universal, and well supported through myriad experimental results. This so-called $-5/3$ behavior, shorthand for $k^{-5/3}$ behavior, can be observed at-a-glance in the frequency domain in fig. 4.2b and wavenumber domain in fig. 4.3a in the candidate measured flowfields. A more rigorous analysis is undertaken by premultiplying the shapes of the u-spectra in ways that better highlight the nature of the distinct regions in the energy cascade. In fig. 4.3b, the u-spectra is premultiplied by dissipation scales and normalized by η to highlight collapse in the high wavenumber regions. This representation is useful in clearly separating the scales in the low-wavenumber domain, where it can be seen that the relative effect of increasing Re_{λ_T} dilates the $-5/3$ region through increased energy transport in the larger eddies of the flow.

The mechanism of generating the relatively large turbulent fluctuations in the flowfields presented herein is accomplished through high local shear rates at the fan array exit plane, particularly evident in the quasi-grid configuration, but also present in the random-phase mode. For turbulent shear flowfields with high local shear rates, the structure of the turbulence exhibits anisotropic tendencies in the direction of downstream evolution. It is useful to capture the principle effects of the mean

shear deformation on the large scale eddies due to the mean velocity gradient. This is accomplished by considering the ratio of the timescales of the small scale turbulent motions to the large eddy mean deformation timescale, as in Lee et al. (1990), which defines a dimensionless shear-rate parameter $S^* = Sq^2/\epsilon$, with $q^2 = u'^2$ and $S = \partial\overline{u}/\partial y$. When displayed in the compensated form of fig. 4.3c (i.e. premultiplied by $\epsilon^{-2/3}(kS^*)^{5/3}$ and plotted in the kS^* domain), the inertial subrange should present horizontally. In this representation it is most readily made apparent the increased subinertial range on account of the increased mean velocity gradients. The two groupings in fig. 4.3c correspond to the R-P mode (lower grouping) and Q-G configuration (upper grouping) and reflect the differences in velocity ratios between adjacent inlet conditions that generate the principle shear layers, as diagrammed in fig. 4.1.

With this picture in mind, the quasi-grid configuration essentially initializes single-stream mixing layers about every edge of the on-off static reconfigurations that evolve and merge with downstream development, likely introducing a spanwise peaked velocity distribution similar to that observed in the freestreams of the mixing layers of Chapter III. Unlike the planar mixing layers with imposed spanwise coherence along the width of the fan array apparatus however, the quasi-grid distribution is broken up along the width and height of the array (symmetrically in this case) and thus introduces three-dimensionality while still maintaining discrete wake-like geometric separations at flow initiation. This is what is meant by a quasi-coherent flow modality. The random-phase configuration, in contrast, allows for temporally-changing inlet conditions at whatever resolution selected. In this way, it is a perturbation technique applicable to any such mean velocity profile that was activated, in this case, at a per-fan basis of a uniform flow modality. Because any given ranged fan input command is phased randomly to its neighbors, velocity differences between adjacent fans are rarely maximum (as in the Q-G case) or zero (adjacent fans of the same velocity) but occupy values in-between according to a Gaussian-like distribution set through software. If the targeted mean velocity is selected to be center of the allowable range, then the bias toward the centered velocities allows for good mean velocity tracking with fluctuations that have no preferred frequency scale. This is what is meant by a pseudo-random flow modality that distributes energy broadly amongst the scales.

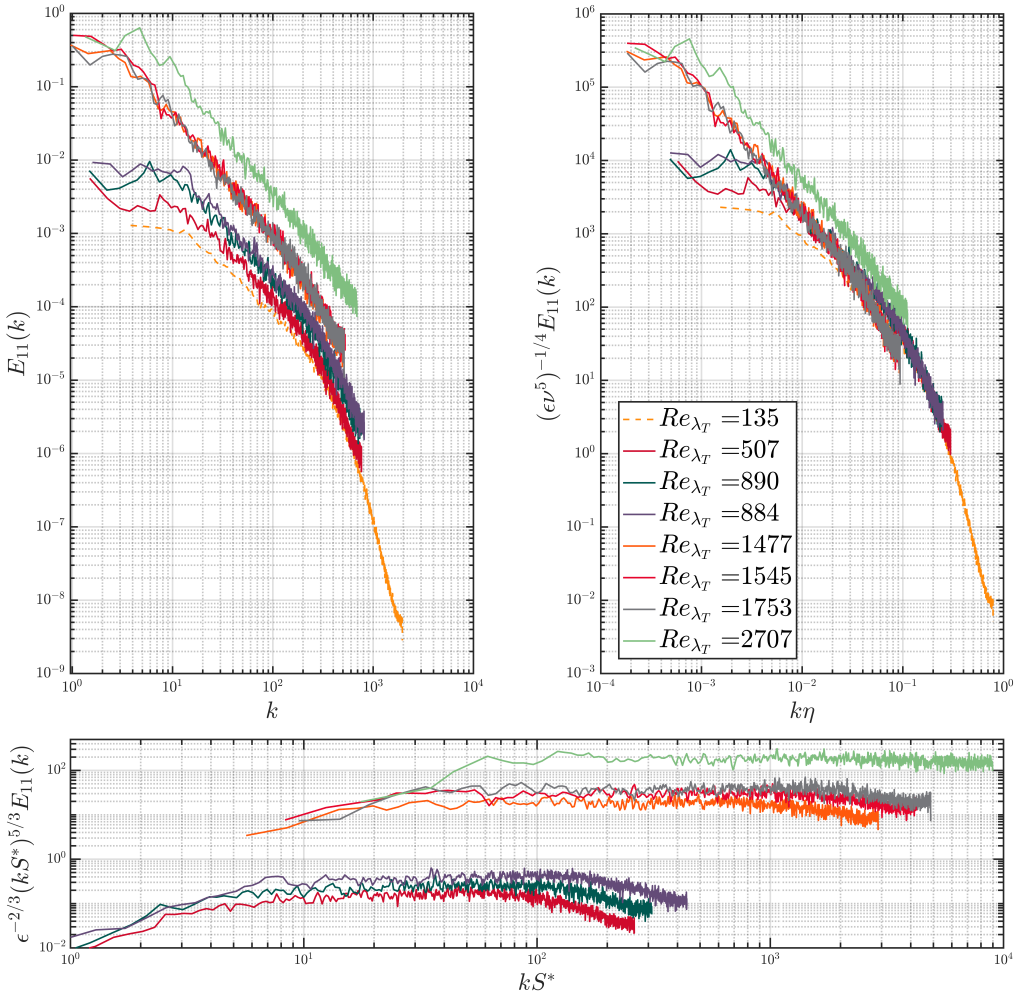

Figure 4.3: The longitudinal velocity (u) spectra with various scalings. The topmost-left is the dimensional u-spectra in the wavenumber domain. The topmost right u-spectra is compensated (pre-multiplied) using the dissipative (Kolmogorov) scales. The bottommost u-spectra is compensated (pre-multiplied) using inertial subrange scales. The Taylor Reynolds number ranges from $Re_{\lambda_T} = 135$ (the baseline uniform case, dashed, with $U = 8.0$ m/s, $TI = 2.7\%$) to $Re_{\lambda_T} = 2707$ (quasi-grid with $U = 9.1$ m/s, $TI = 26.9\%$).

4.4 Summary

In this chapter, turbulence generation techniques based on shearing velocities phased randomly (R-P) and distributed in a grid-like manner (Q-G) are explored in some depth. Based on the results of fig. 4.3 and fig. C.1, the R-P configuration appears to be a good candidate for the generation of pseudo-random atmospheric-like turbulence (of a relevant turbulence intensity) found in the ISL in the frequency range comprising the spectral overlap for flyers of interest. The quasi-grid (Q-G) configuration introduces static initial shear layer conditions (by virtue of forcing a geometric separation at the exit plane) that evolve shear layers into a superimposed three-dimensional wake-like flowfield. Though no statement on spatial structure can be provided at this time, significant increases in velocity fluctuations of the quasi-coherent flow modality at the single-point measurement location compared to the pseudo-random flow modality are noted, as is evident from the values of Re_{λ_T} which were reported as high as $Re_{\lambda_T} \sim 2700$ for the (Q-G) case and ranged from $500 \lesssim Re_{\lambda_T} \lesssim 900$ for the (R-P) case. It can be said that the quasi-coherent flow modality effectively increases u' at the likely expense of flow uniformity through the coarsening static reconfiguration of initial fan RPM distribution. Though no traversals have been reported, one can imagine a significant wave-like appearance to the velocity profiles along the transverse planes not unlike what is observed in the freestream of the mixing layers due to the module geometry funneling effect discussed in Chapter III. These flowfields at the single point measured behave locally isotropically and a general trend of increasing turbulence intensity within groupings is also observed to further dilate the subinertial range. The largest subinertial range is nearly two decades when $Re_{\lambda_T} \sim 2700$, thus confirming that turbulence generated from increased local mean velocity gradients is an effective technique to increase Re_{λ_T}. A more quantitative statistical analysis that promotes comparison of the many flow modalities so far introduced is undertaken next in Chapter V.